PAPER

Check for updates

Additive manufacturing of LiCoO$_2$ electrodes *via* vat photopolymerization for lithium ion batteries

Ana C. Martinez, [ID] *[a] Ana P. Aranzola, [ID] [a] Eva Schiaffino,[a] Eric MacDonald [ID] *[ab] and Alexis Maurel [ID] *[a]

Additive manufacturing has the potential to revolutionize the fabrication of lithium-ion batteries for a diversity of applications including in portable, biomedical, aerospace, and the transportation fields. Standard commercial batteries consist of stacked layers of various components (current collectors, cathode, anode, separator and electrolyte) in a two-dimensional manner. By leveraging the latest advances in additive manufacturing and computer-aided design, an improved geometric and electrochemical configuration of these batteries can maximize energy efficiency while allowing design optimization to reduce dead space for a given application. In this work, a composite UV photosensitive resin was prepared and used as feedstock in a vat photopolymerization system. The resin was loaded with LiCoO$_2$ acting as electrochemically active material for the cathode of a lithium-ion battery, and was further improved with the addition of conductivity-enhancing carbonaceous additives. Challenges to additive manufacturing arise from the opacity and high viscosity of the composite nature of these electrochemically-active resins, which cause light refraction during selective UV curing. Subsequently, items were printed and subjected to a thermal post-processing step to obtain an adequate compromise between electrochemical performance and mechanical integrity. Both sintered and green state 3D printed cathodes were assembled into half-cell lithium-ion batteries using lithium metal as a reference and counter electrode. Electrochemical cycling of these batteries yielded satisfactory results approaching commercial LiCoO$_2$ cathodes' performance, with the potential advantages of additive manufacturing – high surface area anode–cathode configurations for power performance as well as shape conformability.

1. Introduction

Lithium-ion batteries are vital and abundant components in everyday electronics. Since their commercialization in the 1990s, the composition of batteries has remained relegated to the geometry of consecutive two-dimensional stacks of anodes, separator/electrolyte, cathodes, and current collectors. These stacks are assembled to fit coin cells, pouch cells, and cylindrical batteries.[1,2] The functioning principle of batteries is based on lithium intercalation/deintercalation from the cathode to the anode by migrating through the electrolyte into the porosity of the electrodes, for the charge, and the inverse process for the discharge. The electron flow through the external circuit between the anode and the cathode enables the conversion of chemical energy to electrochemical energy.[3,4] This work focuses on a cathode material, LiCoO$_2$, the preferred choice for

batteries targeting consumer portable electronics, due to its high specific energy.[5]

In order to store more energy from existing battery chemistries, a substantial effort has been recently focused on manufacturing intricate 3D anode–cathode architectures, thus increasing the power density by increasing the specific surface area and promoting 3D lithium ion diffusion across the electrodes with increased surface area.[6–10] The limitation of this 3D approach remains in the manufacturing, which is often spatially complex and difficult, if not impossible, for mainstream methods. Additive manufacturing appears in this context to be an exceptional tool to comply with the requirements of 3D battery production by providing complex geometries and toolless manufacturing.[11–16] Among the various additive manufacturing processes, material extrusion using either thermoplastic filaments[11,12,17–20] or inks[21–24] as material feedstock for the 3D printer have been previously studied to manufacture battery components. On the other hand, vat photopolymerization (VPP), another additive manufacturing subcategory, is particularly promising for energy storage applications as this process can provide resolution ranging from as high as 100 μm down to

[a] *Department of Mechanical Engineering, The University of Texas at El Paso, El Paso, TX 79968, USA. E-mail: acmartinezm@utep.edu, amaurel@utep.edu*

[b] *Manufacturing Science Division, Oak Ridge National Laboratory, Oak Ridge, TN 37830, USA*

as low as 100 nm,[25,26] but has often been disregarded for the printing of the electrodes. VPP is a layer-by-layer curing approach that solidifies a liquid UV-photosensitive resin composed of a mixture of polymers and photoinitiators. In order to produce an electrochemically-active structure, solid or soluble battery materials must also be added.[27,28] Solid particles, especially those within the nanometric scale, may scatter or prevent the absorption of the UV light used to cure the composite resin.[29] Therefore, layer thickness, exposure time, temperature, and brightness of the UV light are variables that should be optimized for each composite resin,[30,31] particularly important to simultaneously provide electrochemical functionality while maintaining printability.

Most 3D printing commercial systems have pre-programmed process parameters specifically optimized for their own commercial resins. Consequently, when new custom composite resins are developed, research must be completed to identify the most appropriate set of printing parameters. This work investigates, in a first instance, the best suited printing parameters for obtaining a dimensionally-accurate green state structure containing $LiCoO_2$ (a well-known active material for the positive electrode in commercial lithium-ion batteries) and conductive carbon additives, followed by an appropriate thermal post-processing step. Secondly, the study will demonstrate the proof-of-concept cycling of such cathodes inside a half-cell lithium-ion battery, by comparing the performance obtained from the green state $LiCoO_2$ cathode, to its sintered counterpart. In this work, for the first time, VPP additive manufacturing of lithium-ion battery electrodes using composite resins as material feedstock directly containing solid particles of electrochemically-active material (here $LiCoO_2$) and conductive additives, is reported and serves to provide the foundations for the additive manufacturing of a multi-material lithium-ion battery.

2. Materials and methods

2.1. Design

Planar discs measuring 12.7 mm in diameter and 0.5 mm in thickness were created using the CAD software, nTopology (nTopology, New York). To further increase porosity and complexity, an additional design with the same dimension was made using a 90% infill with a tetrahedral octagonal vertex centroid lattice. The CAD files were converted to Standard Tessellation Language (STL) files utilizing a mesh from an implicit body in nTopology. These files are a composition of colorless triangles to describe the surface of the geometry created[32] and were sliced by the printer software to project 2D UV light images directly to the resin for solidification. Finally, a more complex 3D structure was created also using nTopology. This disc measuring 12.7 mm in diameter and 3 mm in thickness was infilled with a gyroid lattice that had a beam thickness of 1.2 mm.

2.2. Resin preparation and additive manufacturing

In this work, three different UV-photocurable composite resins have been developed to be used as material feedstock in a vat photopolymerization 3D printer:

The first resin, referred to in the text as "control" composite photosensitive resin, was prepared by mixing a commercially available Genesis base resin (Tethon 3D, USA) and $LiCoO_2$ (99.8%, Sigma Aldrich) in a 85:15 wt% ratio. This resin (as well as the two other subsequent composite resins) was employed as feedstock material and tested with the direct light processing (DLP) technique on a Bison 1000 printer (Tethon 3D, USA) equipped with a 405 nm wavelength. The "control" resin was specifically developed with the aforementioned ratio to ensure good printability. Indeed, a compromise must be reached between the printability (provided by the acrylate base resin) and the electrochemical performances (provided by the $LiCoO_2$ loading). A too high amount of $LiCoO_2$ will have a detrimental effect on the printability. It is important to note that the resulting printed electrode from this "control" resin is not yet functional as a cathode due to the lack of conductive carbon black additives. Printing parameters were deduced according to the material's properties as follows: UV light brightness 400 mW cm^{-2}, initial and basic exposure time 45 s, and layer thickness 100 microns. The heat feature was not utilized.

The second resin, referred to in the text as "primary" composite photosensitive resin, contains Genesis base resin and a mixture of $LiCoO_2$ with conductive carbon black Timcal Super C45 (BET = 45 m^2 g^{-1} and 20 nm particle size, MSE Supplies); in a 70:28:2 wt% ratio. The conductive additives were premixed with $LiCoO_2$ in a mortar prior to introduction into the base resin to ensure thorough mixing. The loadings of $LiCoO_2$ and conductive carbon black were here maximized to allow printing of flat patterns while also demonstrating acceptable electrochemical performances for the green state electrodes (without additional thermal post-processing step). Printing parameters on the same DLP printer were set as follows: UV light brightness 750 mW cm^{-2}, initial exposure time 250 s, basic exposure time 70 s, and layer thickness 100 microns. To account for the material's high viscosity, the heater was set to maintain the printer in a range from 35 °C to 50 °C.

Finally, the third resin, referred to in the text as "experimental" composite photosensitive resin, was prepared by mixing Genesis base resin, $LiCoO_2$ and C45 in a 95:4.7:0.3 wt% ratio. Here again, the conductive additives C45 were premixed with $LiCoO_2$ in a mortar prior to introduction into the base resin to ensure thorough mixing. This resin was specifically developed to allow the printability of complex 3D structure (thanks to a higher loading of Genesis base resin polymeric matrix), and at the detriment of the electrochemical performances (due to the lower amount of $LiCoO_2$ active material and conductive additives). The printing parameters on the DLP printer were set as follows: UV light brightness 730 mW cm^{-2}, initial exposure time 70 s, basic exposure time 65 s, layer waiting time 75 s and layer thickness 100 microns. The heat feature was not utilized.

Prior printing, all composite resins were stirred at room temperature in a hot plate for 1 hour, in order to ensure homogeneity and limit the stratification of the fillers within the resins.

2.3. Materials characterization

Thermogravimetric analysis-mass spectrometry (TGA-MS) was executed by means of an STA 449F3 instrument (NETZSCH,

Germany) placed inside an argon-filled glove box (O_2 and H_2O < 0.1 ppm, Jacomex). The experiments were performed from 25 to 900 °C at a rate of 10 K min^{-1} under Ar flow. X-ray powder diffraction (XRD) diffractograms were acquired with an Empyrean-2 X-ray diffractometer (Malvern Panalytical, UK) using Cu Kα radiation (λ = 1.5418 Å), 45 kV of accelerating voltage, and a current of 40 mA. Data was recorded from 10 to 90° 2theta with a step size of 0.013° and scan rate of 8° min^{-1}. Images of the 3D printed items were obtained using an S-4800 (Hitachi, Japan) field emission scanning electron microscope (SEM) operating in high vacuum mode. Secondary electron images were recorded at a maximum 15 kV of acceleration voltage. The green state cathode electrode was frozen on liquid N_2 to obtain a clean cut for the cross-sectional images.

2.4. Lithium-ion battery testing

Green state or sintered 3D-printed cathodes were placed as working electrodes for power performance battery testing. Coin cells were assembled inside an argon-filled glovebox (H_2O < 0.1 ppm, O_2 < 0.1 ppm) using lithium metal (0.38 mm thick ribbon, 99.9% purity, Sigma Aldrich) as a counter and reference electrode. A fiberglass separator (Whatman GE Healthcare) impregnated with 150 μL of 1 M LiPF$_6$ in ethylene carbonate and dimethyl carbonate (EC : DMC 1 : 1 wt, Sigma Aldrich) was used as a separator/liquid electrolyte. The resting time to allow electrolyte impregnation was 13 h. The cells were galvanostatically charged and discharged in a potential window of 2.5–4.3 V *vs.* Li/Li$^+$ for five cycles at C/50, C/20, C/10, and 10 cycles at C/50 (5.48, 13.7, 27.4 and 5.48 mA h g$_{LiCoO_2}$$^{-1}$, respectively), by means of a LBT galvanostat (Arbin, USA). The current densities were calculated considering total lithium extraction (*i.e.* x = 1 in Li$_{1-x}$CoO$_2$).

3. Results and discussion

All composite photocurable resins presented dark coloring typical of the powder materials which blocked UV rays from permeating the resin, thus hindering the increase of the thickness of the objects as well as making harder to adhere to the build plate. Another consequence from the presence of a high powder loading was the increased light scattering. This implies that the UV-light paths were constantly interrupted by the particles thus slowing the photopolymerization process, causing failure to stick to the build plate, undesired macro porosity and defects on the prints. The printing parameters were set to effectively minimize the effect of these issues that are known to prevent the printing of highly loaded resins. It was also observed that when the resins were left untouched, they presented solids sedimentation on the resin tank. To minimize this effect and ensure the correct solid loading was present on the prints, the resins were used immediately after agitation during 1 hour, and the printing of the discs described in the Materials and Methods section did not exceed 7 minutes for the control and primary resins, and 30 minutes for the experimental resin.

During the printing process, the control resin (loaded exclusively with LiCoO$_2$ and without any carbon additives) successfully adhered to the build plate, achieving a maximal thickness of 230 μm. The LiCoO$_2$ particles employed exhibit diameters between 5–15 μm. Upon the addition of nanosized carbon black C45 (primary resin), the UV light permeation is worsened and consequently the adhesion of the initial layers to the build plate is more complicated. Indeed, the discs printed with the primary resin required an increase to the vat temperature, brightness, and initial and basic exposure times to produce adequate prints (Fig. 1a and b).

On both printed discs with different infill, the side of the 3D printed layer facing the tank's film always presented different surface morphology in comparison with the opposite side. In essence, the first layer appeared smoother than the last and important microporosity can be observed on the vat-facing surface (Fig. 2a and b). The surface rugosity became more evident when the cross-section was examined by SEM (Fig. 2c), as some particles appeared almost detached from the print. It is relevant for 3D printed battery components to study these surface features since a low contact rate between the electrodes and the current collector, and a high interfacial rugosity between electrodes and electrolyte (especially when using solid electrolytes) will increase the contact resistance and thus battery impedance.[33,34] The particles are mainly located on the bottom part (vat-facing print surface), whereas the polymer is more visible closer to the plate-facing print surface. This is due to the effect of gravity on the particles within the resin. As it is undesirable for this application to include viscosity-stabilizer additives into the composite resin because of their potential electrochemical activity, it would be interesting to study the effect of a microgravity environment on the printing of highly-loaded additive-free composite resins, as it has been done before for material extrusion,[35] but never for VPP.

On the other hand, the microporosity observed on the vat-facing side is a beneficial feature due to faster electrolyte impregnation when employing liquid electrolytes (the case of this work). Therefore, it was decided that for battery testing the smoother side would face the current collector, whereas the rougher side would face the separator/electrolyte.
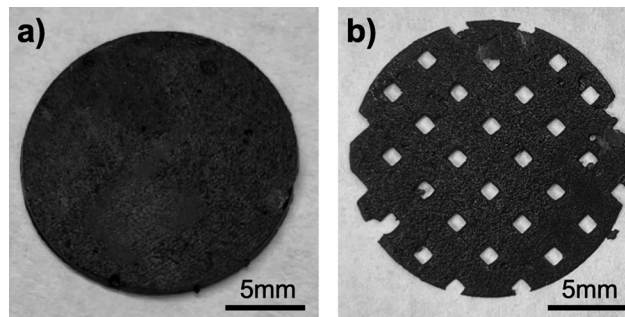

Fig. 1 (a) Picture of the actual 100% infill printed disc from the primary resin and (b) of the 90% infill. The diameter corresponds to the size of a coin cell battery used for electrochemical characterization.
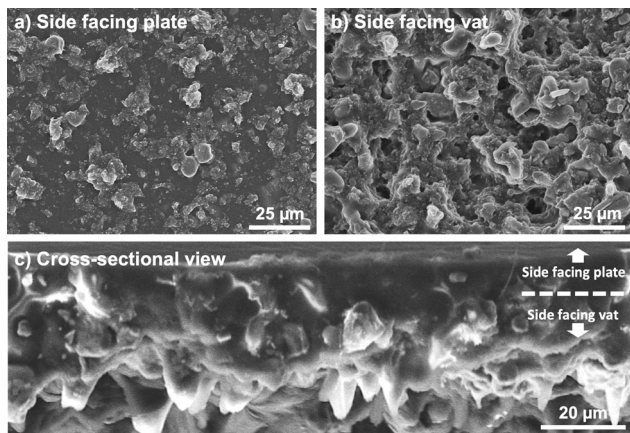
Fig. 2 Top-view SEM images of a green state electrode from (a) the side facing the building plate, and (b) side facing the vat. (c) Cross-sectional view of the printed $LiCoO_2$ electrode.

In spite of the thermal post-processing profiles for battery materials previously published,[14,36] previous profiles cannot be applied to this composite resin because: (i) the composition of the polymeric matrix is not the same, so the debinding step should change, (ii) the sintering temperature is dependent upon the interactions between the solid particles of the mixture, and (iii) it may occur that the solid particles act as retardant/accelerator of the thermal reaction. For this reason, TGA-MS and XRD were used to determine the best thermal profile that eliminates the electrochemically inactive polymeric material, and that at the same time does not alter the crystalline phase of $LiCoO_2$.

TGA-MS analysis of a green state 3D printed piece (from the primary resin) was performed in air from 25 °C to 900 °C and is shown in Fig. 3a. A mass loss of about 60% occurred from 200 °C to 470 °C with two exothermic DTG peaks centered at 340 °C and 415 °C, and a simultaneous production of CO_2 and H_2O gasses as observed in the MS graph. This is associated with the combustion of the polymeric resin in two steps, as it can be seen in the thermal TGA-MS of pure Genesis base resin

(Fig. 3b). By comparing both graphs, it can be deduced that the presence of solid particles in the base resin did not greatly affect the decomposition temperatures, contrary to what was observed before by Martinez et al.[14] when using reactive precursors within the resin. Since the precise chemical composition of the commercial Genesis base resin is a commercial secret, the two other thermal decompositions that occurred at 500 °C and 560 °C can be attributed to the combustion of residual resin products that evolve CO_2 and H_2O gasses, and a part of CO_2 gas stemming from the partial oxidation of the carbon black C45. The green state sample weight did not change after 650 °C, indicating that the polymer combustion was completed by this temperature. The remaining mass was 26%, which corresponds very closely to the amount of $LiCoO_2$ that was added within the primary resin (28%). The slight difference might come from the homogeneity of the resin and sedimentation problems that the printer can face.

XRD analysis of the resulting sintered cathode corroborated that the $LiCoO_2$ material kept its pure composition and did not undergo lithium volatilization (Fig. 4a). Based on these analyses, a thermal post-processing profile was designed (Fig. 4b). It consisted of heating at a rate of 1 °C min^{-1} until 300 °C to remove residual water, immediately followed by heating at 0.2 °C min^{-1} until 400 °C (matching the DTG peak) and holding for two hours to prevent cracks formation during the polymer combustion. Then the temperature was increased at the same speed until 550 °C and then until 600 °C (matching the broad DTG peaks in the 500–600 °C zone that corresponds to the polymer derivatives degradation), where the temperature is held for two hours and one hour, respectively. Finally, the temperature was increased at the fast rate of 4 °C min^{-1} and held at 750 °C for four hours to promote particle sintering. Note that by the end of the sintering profile integral sintered pieces were difficult to obtain because a solid loading below 50% usually presents excessive shrinkage and delamination issues during debinding and sintering steps.[37]

A closer SEM view to the surface microstructure of the green state electrode printed from the primary resin and the
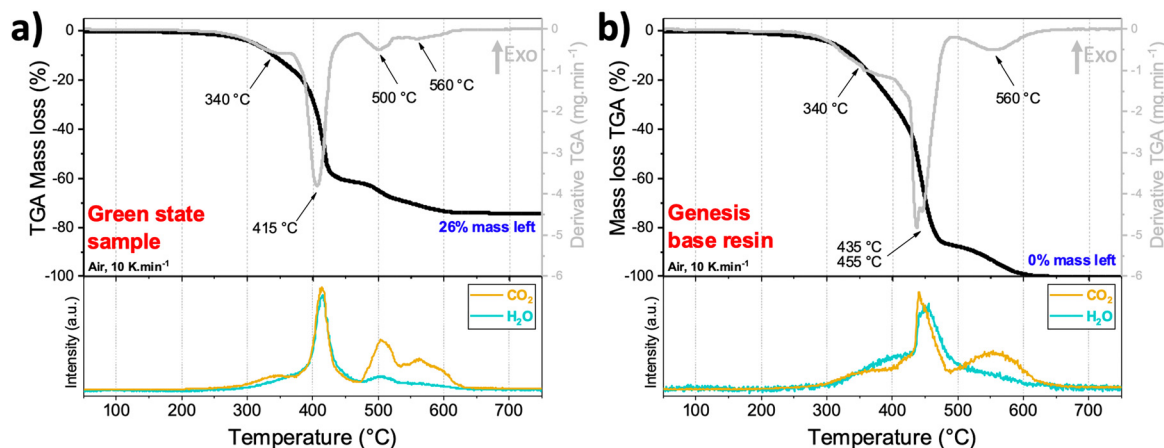

Fig. 3 (a) TG (top) and MS (bottom) analysis of the composite resin containing $LiCoO_2$ and carbon black C45 materials in the green state (before thermal post-processing). (b) TG (top) and MS (bottom) analysis of the Genesis base resin.
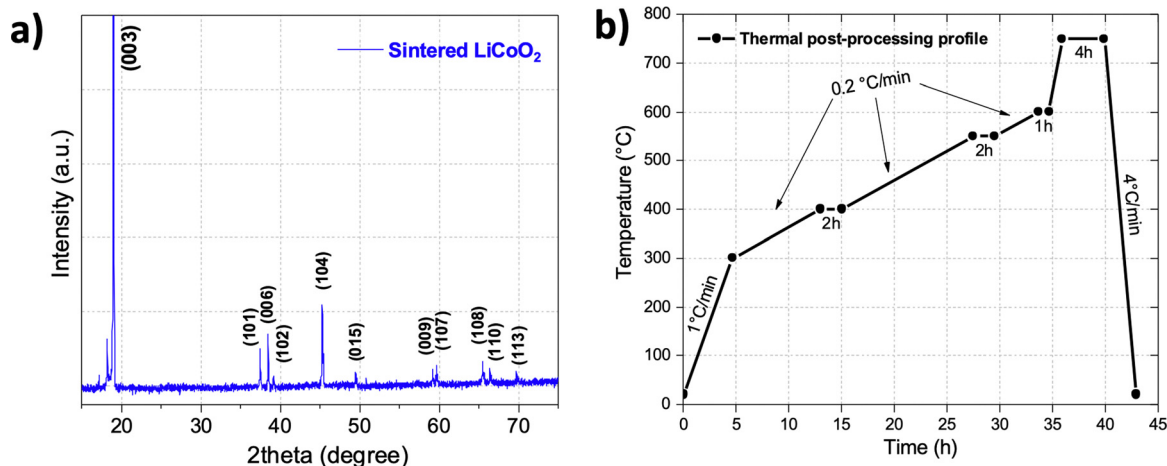
Fig. 4 (a) XRD diffractogram obtained from the residues left from thermal post-processing. The reflections of $LiCoO_2$ are indicated in parentheses. (b) Thermal post-processing profile including debinding and sintering steps.

corresponding sintered electrode, revealed that surprisingly the green state electrode (side facing vat) presents microporosity desired for battery function (Fig. 5a). Most importantly, the thermal post-processing step kept this microporosity (Fig. 5b), while also having little effect on the sintering of the particles, which is important to control so that the channels for electrolyte impregnation are kept (Fig. 5c and d). A comparison with the bare $LiCoO_2$ particles showed that the particles did not change their morphology after heating at a maximum temperature of 750 °C during four hours, as it was also recently observed by Valera-Jiménez et al.[36] after the sintering at a maximum temperature of 900 °C for six hours of a printed item obtained via thermoplastic filament extrusion containing $LiCoO_2$ particles.

The initial charge capacity of the green state sample printed from the primary resin was 62 mA h $g_{LiCoO_2}^{-1}$ in half-cell battery configuration at a C-rate of C/50 (Fig. 6a). This capacity value is surprisingly high since the amount of electrochemically inactive resin is high (70 wt%). Nonetheless, it is still far from the practical capacity of $LiCoO_2$ electrodes with an upper cut-off voltage of 4.3 V vs. Li/Li$^+$: 155–165 mA h $g_{LiCoO_2}^{-1}$.[38] The discrepancy between practical and observed capacity can be explained by the polymeric matrix resin which is not electrically nor ionically conductive, and therefore creates a resistance that prevents lithium and electrons conduction. The presence of a polarization resistance in the green state electrode can also be observed in the potential gaps between the main peaks on the dQ/dV plot (Fig. 6b). Both curves in Fig. 6b exhibit a pair of main redox peaks between 3.85–3.95 V vs. Li/Li$^+$, corresponding to the first-order phase transition of $LiCoO_2$ upon lithiation and delithiation. The other two redox peaks result from phase transitions between ordered and disordered Li$^+$ arrangements in the CoO_2 framework.[39] The potential gap between the main redox peaks is bigger in the green state electrode ($\sim$50 mV), than in the sintered electrode ($\sim$20 mV); and the peaks of the green state electrode are not as sharp and pronounced as for the sintered electrode. This means that the green state electrode presents higher polarization resistance to the flow of lithium ions. An analysis of the specific capacity versus potential plots also revealed that the charge and discharge curves of the green state electrode do not present a clearly defined plateau around 3.9 V vs. Li/Li$^+$, typically attributed to polarization resistance (Fig. 6c). Upon further cycling at C/20 and C/10 that delivered low specific discharge capacity values (32 mA h $g_{LiCoO_2}^{-1}$ and 19 mA h $g_{LiCoO_2}^{-1}$, respectively), the initial capacity values at C/50 were recovered partially from cycle #15 (40 mA h $g_{LiCoO_2}^{-1}$). The data indicates that the green state electrode is capable of retaining and delivering at least 65% of the initial electrochemical energy in the presence of a high amount of inactive polymer for at least 25 cycles. In a future work, a flexible composite resin could be designed to 3D print analogous battery electrodes, thus potentially making them suitable for deployment in areas that require flexibility, such as soft sensors and soft robotics.

In the literature, Maurel et al.[12] also reported an adequate electrochemical performance from a green state $LiFePO_4$-based
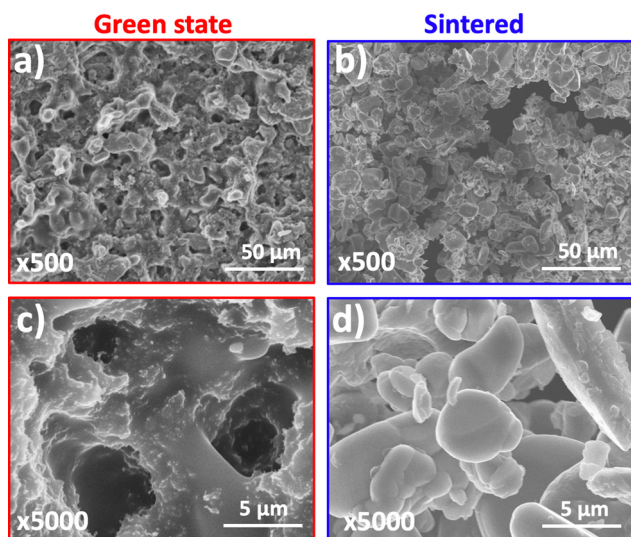

Fig. 5 (a)–(d) SEM images of the printed pieces in the green (side facing vat) or sintered states.
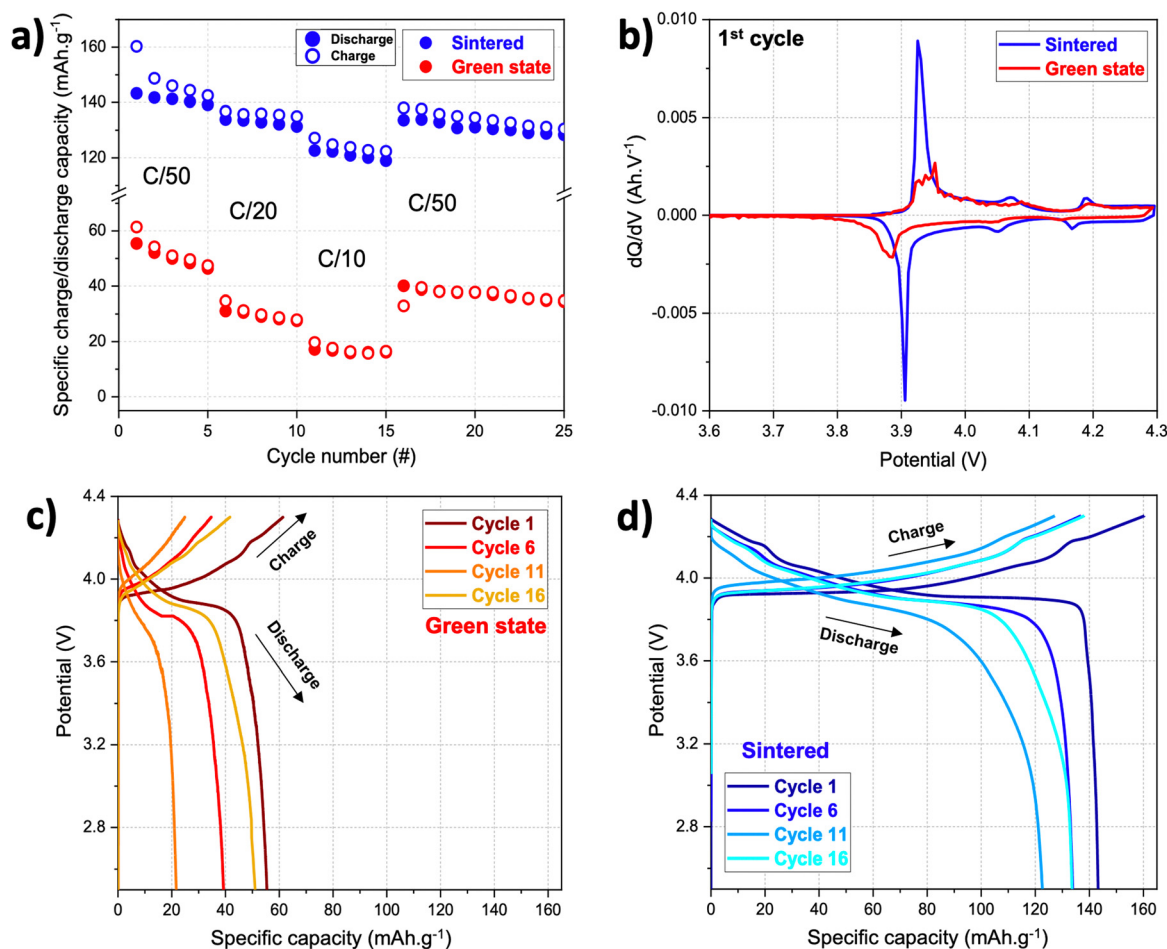
Fig. 6 Battery testing for the green state and sintered electrodes in the form of (a) power performance tests, (b) dQ/dV plots, and (c) and (d) potential *versus* specific capacity plots.

cathode printed *via* fused deposition modeling. For the cathode containing 33 wt% of polymers, they reported a specific discharge capacity of 90 mA h g^{-1} at C/20 (56% of the practical capacity). From the same group, Maurel *et al.*[40] recently reported a green state TiO$_2$-based VPP printed electrode exhibiting low specific capacity when cycled *versus* Na/Na$^+$ ($<$10 mA h g^{-1}). However, upon sintering in argon, high specific capacities of 60 and 115 mA h g^{-1} *versus* Na/Na$^+$ and Li/Li$^+$, respectively were achieved. In a related work, Valera-Jimenez *et al.*[36] demonstrated the debinding and sintering of LiCoO$_2$-based electrodes printed *via* thermoplastic extrusion AM. For a LiCoO$_2$ electrode sintered at 900 $^\circ$C in N$_2$ and cycled at C/10, they reported an average reversible capacity of 129 mA h g^{-1} (205 mA h cm^{-3} for the total volume electrode), which corresponds to 81% of the practical capacity of LiCoO$_2$. These works demonstrate the importance of thermal post-processing to improve the electrochemical performance of printed electrodes.

After thermal post-processing, our LiCoO$_2$-based electrode exhibited higher specific capacities than the green state electrode. Fig. 6a shows the electrochemical performance of the sintered LiCoO$_2$-based cathode that was sufficiently mechanically stable to be tested in coin cell battery configuration. This electrode delivered 160 mA h g$_{\text{LiCoO}_2}^{-1}$ in the first discharge, a

value close to the commercial performance of LiCoO$_2$, and an irreversible capacity loss from the first charge to the second of only 7% (in comparison with 12% from the green state electrode). The initial irreversible capacity is due to a combination of the loss of lithium sites due to irreversible structural changes on LiCoO$_2$, the parasitic electrochemical reactions occurring on the surface of the electrode with the electrolyte, and the slow kinetics for lithium intercalation.[41] While the first two are irreversible, the last is mainly dependent on temperature and current density. In 3D printed electrodes, the main cause for large initial irreversibility is often the parasitic electrochemical reactions due to the use of polymer matrices and thermal post-processing steps that affect the purity of a printed electrode. Upon further cycling, the discharge capacity decreased to 134 mA h g$_{\text{LiCoO}_2}^{-1}$ and to 123 mA h g$_{\text{LiCoO}_2}^{-1}$ when cycling at C/20 and C/10, respectively; but 128 mA h g$_{\text{LiCoO}_2}^{-1}$ of discharge capacity were still recovered at C/50 after 25 cycles (around 80% of the practical capacity of LiCoO$_2$). Individual potential *versus* specific capacity plots illustrating the charge and discharge profiles are shown in Fig. 6d. In this case, the curves are more defined and clearer plateaus can be observed around 3.9 V *vs.* Li/Li$^+$.

The electrochemical results shown in this work (for the green state and sintered cathodes obtained from the primary

resin) compare with the precursor approach that has been recently used to develop a LiCoO$_2$ cathode for lithium-ion battery application.[14,42] In this reported method, lithium and cobalt precursor salts were dissolved into the photocurable resin. The lack of solid particles in the feedstock material benefited the printing process by avoiding particle light scattering and allowed the printing of more complex geometries. However, disadvantages to this method correlate to the lack of electronic conductivity as electrode materials are very often poorly conductive oxides. As stated in this work, the addition of conductive carbon in powder-based resins enabled the electrochemical cycling of a green state electrode (at the expense of low capacity), whereas green state electrodes printed from precursor resins simply cannot deliver electrochemical functionality because of the absence of LiCoO$_2$ active material.

In a separate experiment, the total amount of solid loading content of LiCoO$_2$ and carbon black C45 in the primary composite resin was reduced from 30 to 4 wt% only; this composite resin is called the experimental resin. The motivation behind this experimental resin is to allow the printability of complex 3D structure or thicker cathode thanks to a higher loading of polymeric matrix, but at the detriment of the electrochemical performances due to the lower amount of LiCoO$_2$ active material and conductive additives. Fig. 7a shows the designed gyroid disc that was printed from the experimental resin. As the total amount of solid particles within the resin was decreased, thus resulting in reduced light scattering during printing, the printability was facilitated and printing parameters such as brightness, initial and basic exposure times were reduced to ensure adequate print quality. Although electrochemical properties were not tested for this printed electrode, it is expected that lower capacity values would be obtained because of the high amount of electrochemically inactive polymer, when compared with the green state cathode printed from the primary resin. This experiment shows the necessity to find a compromise between printability and electrochemical performance.

In retrospect, the issues related to particle sedimentation and opacity can be minimized through four procedures: (i) the modification of the resin formulation, (ii) the implementation of a start-and-stop method for changing the resin within the tank, (iii) the usage of an alternate printer, and (iv) printing under a microgravity environment. The former includes using viscosifiers, dispersants, and additives; but is not preferred because of their potential electrochemical activity. The implementation of a start-and-stop method to change the resin is particularly relevant for larger and vertically extended components. Alternate printers equipped with a recirculation system of the feedstock appear as a more fitting option to avoid sedimentation issues. On the other hand, it is expected that microgravity will improve the homogeneity of 3D printed battery components and their resulting electrochemical performances by benefiting both the head pressure and particle distribution. The effect of gravity on particle sedimentation during the additive manufacturing material extrusion process has been studied on the International Space Station (ISS) previously,[35] however, it remains a challenge to further validate for the VPP processes targeting battery functionality.

4. Future outlook

The development of complete complex battery architectures using the software Fusion 360 was explored. With the aid of computer visualization and design, innovative battery geometries increasing in complexity can be created to analyze the efficiency of the investigated parameters. An example of explored geometries is shown in Fig. 7b, where three intertwined helices corresponding to cathode, anode and solid electrolyte assemble together to form the complete battery. In this design, it is envisaged that the current is collected by tab collectors produced on the outside shape through ink writing. Another option is the current being collected by a specific case design containing metal parts that fit each electrode surface. It is expected that in the near future a VPP multi-material printer will facilitate the assembly of all battery components into one single print.[43–46] Ultimately, these 3D-printed batteries could power actuators (i.e. shape memory alloys), for the fabrication by means of additive manufacturing of fully printed soft robots.[47–49] Printed batteries could also be seamlessly integrated within the frame of various objects (i.e. smartwatches, smart glasses, or satellites), to serve as structural batteries with dual energy storage and load-bearing capabilities, utilizing the space within objects that would normally go unused, such as the space within the wristband of a smartwatch or frame of a satellite, for housing the batteries.[27,46]
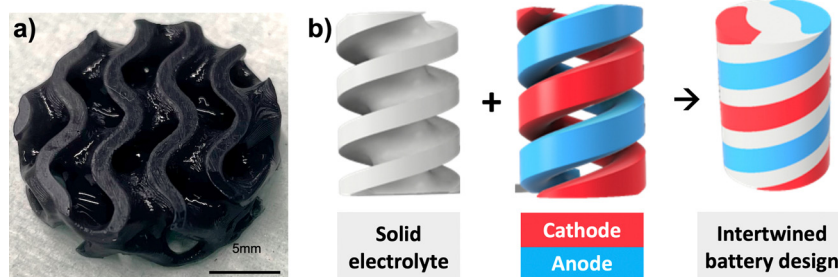

Fig. 7 (a) Gyroid thick cathode electrode printed from the experimental resin. (b) Example of envisaged multi-material structures that could be printed with a multi-material printer.

5. Conclusion

In this work, for the first time, the preparation and VPP additive manufacturing of a composite UV photosensitive resin, loaded with solid particles of active material and conductive additives, and specifically designed to print a cathode electrode of a classical lithium-ion battery, was performed. The resin was loaded with $LiCoO_2$ acting as cathode electro-active active material. $LiCoO_2$ cathodes were printed using a low-cost desktop DLP printer, in which the printing parameters were carefully selected considering that the opacity and viscosity of the resins hinder the 3D printing. It was found that electrodes printed from composite resins present certain inhomogeneity that may impact the electrochemical results because of sedimentation issues. Then, through an adequate thermal profile deduced from TGA-MS data, a sintered electrode delivered electrochemical specific capacity close to the commercial value for $LiCoO_2$-based batteries. Surprisingly, the green state item also showed electrochemical activity, which we attributed to the certain microporosity created during printing. Finally, this work serves as a reference for future efforts to 3D print composite materials with similar high loading of solid particles, and invites the research community to invest time in the design, printing, and optimization of battery components tailored with complex shapes, allowing the future direct incorporation of batteries within complex 3D objects.

Author contributions

ACM and AM contributed to paper conceptualization, formal analysis, investigation, methodology, supervision, validation, visualization, writing – original draft, and writing – review & editing. APA and ES contributed to investigation, methodology, data curation, and writing – original draft. EM contributed to supervision, validation, resources, funding acquisition, and writing – review & editing.

Data availability

The data that support the findings of this study are available from the corresponding author upon reasonable request.

Conflicts of interest

There are no conflicts to declare.

Acknowledgements

References

1 J. K. Par, *Principles and Applications of Lithium Secondary Batteries*, John Wiley & Sons, 2012, p. 380. Available from: **https://play.google.com/store/books/details?id=papHH-urMVYC**.

2 A. A. Franco, *Rechargeable Lithium Batteries: From Fundamentals to Applications*, Elsevier, 2015, p. 412. Available from: **https://play.google.com/store/books/details?id=eUSdBAAAQBAJ**.

3 M. Broussely, P. Biensan and B. Simon, Lithium insertion into host materials: the key to success for Li ion batteries, *Electrochim. Acta*, 1999, **45**(1), 3–22. Available from: **https://sciencedirect.com/science/article/pii/S0013468699001899**.

4 G. Zubi, R. Dufo-López, M. Carvalho and G. Pasaoglu, The lithium-ion battery: State of the art and future perspectives, *Renewable Sustainable Energy Rev.*, 2018, **89**, 292–308. Available from: **https://www.sciencedirect.com/science/article/pii/S1364032118300728**.

5 Y. Lyu, X. Wu, K. Wang, Z. Feng, T. Cheng and Y. Liu, *et al.*, An overview on the advances of LiCoO 2 cathodes for lithium-ion batteries, *Adv. Energy Mater.*, 2021, **11**(2), 2000982. Available from: **https://onlinelibrary.wiley.com/doi/abs/10.1002/aenm.202000982?casa_token=cm7bwWHbwCYAAAAA:2QJZD72V_Vyltdw1jYodK0i2_jJe1lKo5Q0qzKrAAdegHQzE3LeaX-51BC6d7-HMBnhylDricUq2oganEpw**.

6 D. Golodnitsky, M. Nathan, V. Yufit, E. Strauss, K. Freedman and L. Burstein, *et al.*, Progress in three-dimensional (3D) Li-ion microbatteries, *Solid State Ionics*, 2006, **177**(26), 2811–2819. Available from: **https://www.sciencedirect.com/science/article/pii/S0167273806001172**.

7 A. A. Talin, D. Ruzmetov, A. Kolmakov, K. McKelvey, N. Ware and F. El Gabaly, *et al.*, Fabrication, Testing, and Simulation of All-Solid-State Three-Dimensional Li-Ion Batteries, *ACS Appl. Mater. Interfaces*, 2016, **8**(47), 32385–32391, DOI: **10.1021/acsami.6b12244**.

8 Y. Liu, D. Lin, Y. Jin, K. Liu, X. Tao and Q. Zhang, *et al.*, Transforming from planar to three-dimensional lithium with flowable interphase for solid lithium metal batteries, *Sci. Adv.*, 2017, **3**(10), eaao0713, DOI: **10.1126/sciadv.aao0713**.

9 J. W. Long, B. Dunn, D. R. Rolison and H. S. White, 3D architectures for batteries and electrodes, *Adv. Energy Mater.*, 2020, **10**(46), 2002457, DOI: **10.1002/aenm.202002457**.

10 D. S. Ashby, C. S. Choi, M. A. Edwards, A. A. Talin, H. S. White and B. S. Dunn, High-Performance Solid-State Lithium-Ion Battery with Mixed 2D and 3D Electrodes, *ACS Appl. Energy Mater.*, 2020, **3**(9), 8402–8409, DOI: **10.1021/acsaem.0c01029**.

11 A. Maurel, M. Courty, B. Fleutot, H. Tortajada, K. Prashantha and M. Armand, *et al.*, Highly Loaded Graphite–Polylactic Acid Composite-Based Filaments for Lithium-Ion Battery Three-Dimensional Printing, *Chem. Mater.*, 2018, **30**(21), 7484–7493, DOI: **10.1021/acs.chemmater.8b02062**.

12 A. Maurel, S. Grugeon, B. Fleutot, M. Courty, K. Prashantha and H. Tortajada, *et al.*, Three-Dimensional Printing of a LiFePO₄/Graphite Battery Cell via Fused Deposition Modeling, *Sci. Rep.*, 2019, **9**(1), 18031, DOI: **10.1038/s41598-019-54518-y**.

13 A. Maurel, A. C. Martinez Maciel, S. Panier, S. Grugeon, L. Dupont and S. T. Sreenivasan, *et al.*, Lithium-Ion Battery 3D Printing: From Thermoplastic Material Extrusion to Vat Photopolymerization Process, *Meet. Abstr.*, 2021, **MA2021-02**(1), 30, DOI: **10.1149/MA2021-02130mtgabs/meta**.

14 A. C. Martinez, A. Maurel, A. P. Aranzola, S. Grugeon, S. Panier and L. Dupont, *et al.*, Additive manufacturing of LiNi$_{1/3}$Mn$_{1/3}$Co$_{1/3}$O$_2$ battery electrode material via vat photopolymerization precursor approach, *Sci. Rep.*, 2022, **12**(1), 19010, DOI: **10.1038/s41598-022-22444-1**.

15 A. Maurel, A. C. Martinez, D. A. Dornbusch, W. H. Huddleston, M. L. Seol and C. R. Henry, *et al.*, What Would Battery Manufacturing Look Like on the Moon and Mars?, *ACS Energy Lett.*, 2023, 1042–1049, DOI: **10.1021/acsenergylett.2c02743**.

16 M. Pei, H. Shi, F. Yao, S. Liang, Z. Xu and X. Pei, *et al.*, 3D printing of advanced lithium batteries: a designing strategy of electrode/electrolyte architectures, *J. Mater. Chem. A*, 2021, **9**(45), 25237–25257. Available from: **https://pubs.rsc.org/en/content/articlehtml/2021/ta/d1ta06683h**.

17 V. Boudeville, S. Grugeon, A. Maurel, R. Lesieur, M. Louati and A. Cayla, *et al.*, Solvent-free extrusion of a LiFePO4-based monofilament for three-dimensional printing of a lithium-ion battery positive electrode, *J. Power Sources*, 2024, **593**, 233973. Available from: **https://www.sciencedirect.com/science/article/pii/S0378775323013496**.

18 A. Maurel, M. Armand, S. Grugeon, B. Fleutot, C. Davoisne and H. Tortajada, *et al.*, Poly(Ethylene Oxide)-LiTFSI Solid Polymer Electrolyte Filaments for Fused Deposition Modeling Three-Dimensional Printing, *J. Electrochem. Soc.*, 2020, **167**(7), 070536, DOI: **10.1149/1945-7111/ab7c38**.

19 C. Reyes, R. Somogyi, S. Niu, M. A. Cruz, F. Yang and M. J. Catenacci, *et al.*, Three-Dimensional Printing of a Complete Lithium Ion Battery with Fused Filament Fabrication, *ACS Appl. Energy Mater.*, 2018, **1**(10), 5268–5279, DOI: **10.1021/acsaem.8b00885**.

20 H. Ragones, S. Menkin, Y. Kamir, A. Gladkikh, T. Mukra and G. Kosa, *et al.*, Towards smart free form-factor 3D printable batteries, *Sustainable Energy Fuels*, 2018, **2**(7), 1542–1549, DOI: **10.1039/c8se00122g**.

21 K. Sun, T. S. Wei, B. Y. Ahn, J. Y. Seo, S. J. Dillon and J. A. Lewis, 3D printing of interdigitated Li-ion microbattery architectures, *Adv. Mater.*, 2013, **25**(33), 4539–4543, DOI: **10.1002/adma.201301036**.

22 K. Fu, Y. Wang, C. Yan, Y. Yao, Y. Chen and J. Dai, *et al.*, Graphene Oxide-Based Electrode Inks for 3D-Printed Lithium-Ion Batteries, *Adv. Mater.*, 2016, **28**(13), 2587–2594, DOI: **10.1002/adma.201505391**.

23 T. S. Wei, B. Y. Ahn, J. Grotto and J. A. Lewis, 3D Printing of Customized Li-Ion Batteries with Thick Electrodes, *Adv. Mater.*, 2018, **30**(16), e1703027, DOI: **10.1002/adma.201703027**.

24 H. Shi, M. Pei, S. Wang, F. Yao, Y. Xia and Z. Xu, *et al.*, 3D-printed periodic hierarchical porous rGO/ti$_3$C$_2$T$_x$ architectures induced uniform lithium deposition for Li metal anodes, *Adv. Mater. Technol.*, 2023, **8**(1), 2200256, DOI: **10.1002/admt.202200256**.

25 G. A. Appuhamillage, N. Chartrain, V. Meenakshisundaram, K. D. Feller, C. B. Williams and T. E. Long, 110th Anniversary: Vat Photopolymerization-Based Additive Manufacturing: Current Trends and Future Directions in Materials Design, *Ind. Eng. Chem. Res.*, 2019, **58**(33), 15109–15118, DOI: **10.1021/acs.iecr.9b02679**.

26 A. C. Martinez, E. M. Schiaffino, A. P. Aranzola, C. A. Fernandez, M. L. Seol and C. G. Sherrard, *et al.*, Multiprocess 3D printing of sodium-ion batteries *via* vat photopolymerization and direct ink writing, *J. Phys. Energy*, 2023, **5**(4), 045010, DOI: **10.1088/2515-7655/acf958/meta**.

27 A. Maurel, A. C. Martinez, S. Grugeon, S. Panier, L. Dupont and P. Cortes, *et al.*, Toward High Resolution 3D Printing of Shape-Conformable Batteries via Vat Photopolymerization: Review and Perspective, *IEEE Access*, 2021, **9**, 140654, DOI: **10.1109/ACCESS.2021.3119533**.

28 A. Al Rashid, W. Ahmed, M. Y. Khalid and M. Koç, Vat photopolymerization of polymers and polymer composites: Processes and applications, *Addit. Manuf.*, 2021, **47**, 102279. Available from: **https://www.sciencedirect.com/science/article/pii/S2214860421004395**.

29 A. Medellin, W. Du, G. Miao, J. Zou, Z. Pei and C. Ma, Vat Photopolymerization 3D Printing of Nanocomposites: A Literature Review, *J. Micro. Nano-Manuf.*, 2019, **7**(3), 031006. Available from: **https://asmedigitalcollection.asme.org/micronanomanufacturing/article-abstract/7/3/031006/955160/Vat-Photopolymerization-3D-Printing-of?redirectedFrom=fulltext**.

30 Z. Chen, X. Song, L. Lei, X. Chen, C. Fei and C. T. Chiu, *et al.*, 3D printing of piezoelectric element for energy focusing and ultrasonic sensing, *Nano Energy*, 2016, **27**, 78–86. Available from: **https://www.sciencedirect.com/science/article/pii/S2211285516302312**.

31 K. Zhang, C. Xie, G. Wang, R. He, G. Ding and M. Wang, *et al.*, High solid loading, low viscosity photosensitive Al$_2$O$_3$ slurry for stereolithography based additive manufacturing, *Ceram. Interfaces*, 2019, **45**(1), 203–208. Available from: **https://www.sciencedirect.com/science/article/pii/S0272884218326154**.

32 STL files explained. Available from: **https://www.adobe.com/creativecloud/file-types/image/vector/stl-file.html**.

33 H. Nara, D. Mukoyama, R. Shimizu, T. Momma and T. Osaka, Systematic analysis of interfacial resistance between the cathode layer and the current collector in lithium-ion batteries by electrochemical impedance spectroscopy, *J. Power Sources*, 2019, **409**, 139–147. Available from: **https://www.sciencedirect.com/science/article/pii/S0378775318309856**.

34 C. Chen, M. Jiang, T. Zhou, L. Raijmakers, E. Vezhlev and B. Wu, *et al.*, Interface aspects in all-solid-state Li-based batteries reviewed, *Adv. Energy Mater.*, 2021, **11**(13), 2003939, DOI: **10.1002/aenm.202003939**.

35 M. Snyder, J. Dunn and E. Gonzalez, The Effects of Microgravity on Extrusion Based Additive Manufacturing. AIAA SPACE 2013 Conference and Exposition, 2013, DOI: **10.2514/6.2013-5439**.

36 J. F. Valera-Jiménez, J. C. Pérez-Flores, M. Castro-García and J. Canales-Vázquez, Development of full ceramic electrodes

for lithium-ion batteries *via* desktop-fused filament fabrication and further sintering, *Appl. Mater. Today*, 2021, **25**, 101243. Available from: **https://www.sciencedirect.com/science/article/pii/S2352940721003061**.

37 S. Zakeri, M. Vippola and E. Levänen, A comprehensive review of the photopolymerization of ceramic resins used in stereolithography, *Addit. Manuf.*, 2020, **35**, 101177. Available from: **https://www.sciencedirect.com/science/article/pii/S2214860420305492**.

38 M. D. Radin, S. Hy, M. Sina, C. Fang, H. Liu and J. Vinckeviciute, *et al.*, Narrowing the gap between theoretical and practical capacities in Li-ion layered oxide cathode materials, *Adv. Energy Mater.*, 2017, **7**(20), 1602888, DOI: **10.1002/aenm.201602888**.

39 B. Shen, P. Zuo, P. Fan, J. Yang, G. Yin and Y. Ma, *et al.*, Improved electrochemical performance of NaAlO2-coated LiCoO2 for lithium-ion batteries, *J. Solid State Electrochem.*, 2017, **21**(4), 1195–1201, DOI: **10.1007/s10008-016-3475-1**.

40 A. Maurel, A. C. Martinez, S. B. Chavari, B. Yelamanchi, M. L. Seol and D. A. Dornbusch, *et al.*, 3D Printed TiO$_2$ Negative Electrodes for Sodium-Ion and Lithium-Ion Batteries using Vat Photopolymerization, *J. Electrochem. Soc.*, 2023, **170**, 100538, DOI: **10.1149/1945-7111/ad0420**.

41 H. Zhou, F. Xin, B. Pei and M. S. Whittingham, What Limits the Capacity of Layered Oxide Cathodes in Lithium Batteries, *ACS Energy Lett.*, 2019, **4**(8), 1902–1906, DOI: **10.1021/acsenergylett.9b01236**.

42 D. W. Yee, M. A. Citrin, Z. W. Taylor, M. A. Saccone, V. L. Tovmasyan and J. R. Greer, Hydrogel-based Additive Manufacturing of Lithium Cobalt Oxide, *Adv. Mater. Technol.*, 2021, **6**, 2000791, DOI: **10.1002/admt.202000791**.

43 J. Wang, X. Huang and J. Chen, Challenge-driven printing strategies toward high-performance solid-state lithium batteries, *J. Mater. Chem. A*, 2022, **10**(6), 2601–2617. Available from: **https://pubs.rsc.org/en/content/articlelanding/2022/TA/D1TA09322C**.

44 F. Zhang, L. Zhu, Z. Li, S. Wang, J. Shi and W. Tang, *et al.*, The recent development of vat photopolymerization: A review, *Addit. Manuf.*, 2021, **48**, 102423. Available from: **https://www.sciencedirect.com/science/article/pii/S2214860421005753**.

45 P. Gonzalez, E. Schwarzer, U. Scheithauer, N. Kooijmans and T. Moritz, Additive Manufacturing of Functionally Graded Ceramic Materials by Stereolithography, *J. Visualized Exp.*, 2019, (143), DOI: **10.3791/57943**.

46 A. Maurel, A. Pavone, G. Stano, A. C. Martinez, E. MacDonald and G. Percoco, Manufacturing-oriented review on 3D printed lithium-ion batteries fabricated using material extrusion, *Virtual Phys. Prototyping*, 2023, **18**(1), e2264281, DOI: **10.1080/17452759.2023.2264281**.

47 G. Stano, S. M. A. I. Ovy, J. R. Edwards, M. Cianchetti, G. Percoco and Y. Tadesse, One-shot additive manufacturing of robotic finger with embedded sensing and actuation, *Int. J. Adv. Manuf. Technol.*, 2023, **124**(1), 467–485, DOI: **10.1007/s00170-022-10556-x**.

48 M. Mohammadi, A. Z. Kouzani, M. Bodaghi, Y. Xiang and A. Zolfagharian, 3D-printed phase-change artificial muscles with autonomous vibration control, *Adv. Mater. Technol.*, 2023, **8**, 2300199, DOI: **10.1002/admt.202300199**.

49 S. Bodkhe, L. Vigo, S. Zhu, O. Testoni, N. Aegerter and P. Ermanni, 3D printing to integrate actuators into composites, *Addit. Manuf.*, 2020, **35**, 101290. Available from: **https://www.sciencedirect.com/science/article/pii/S221486042030662X**.